

APPLICATION OF ARTIFICIAL NEURAL NETWORK FOR THE IONIZING RADIATION PARTICLE IDENTIFICATION BY THE PLASTIC SCINTILLATION DETECTOR RESPONSE

J. Garankin and A. Plukis

Center for Physical Sciences and Technology, Savanorių 231, 02300 Vilnius, Lithuania

Email: jevgenij.garankin@ftmc.lt

Received 6 June 2022; revised 31 July 2022; accepted 13 September 2022

The separation of ionizing radiation particles is an important and challenging task, especially regarding neutrons and gamma rays. The separation of neutron and gamma radiation is necessary for safeguard purposes and control of nuclear reactions. Standard mathematical models of pulse analysis work well in the presence of large energy transfer (>1 MeV) from the particle to the detector. However, the quality of the separation decreases as the amount of transferred energy lessens, making it impossible to determine the exact type of particle at a sufficiently low-energy level.

In this work, an artificial neural network model was used to solve the problem of separation at low-energy levels. The supervised machine learning (ML) model was used to analyse pulses received from the polyethylene naphthalate (PEN) scintillation detector. Several data sets after the PEN exposure to neutron/gamma (combined $^{239}\text{PuBe}$ and $^{238}\text{PuBe}$ source), alpha (^{238}Pu) and beta ($^{90}\text{Sr}/^{90}\text{Y}$) sources were used to train the models. The information obtained from the separation of neutrons and gamma particles was compared with the information obtained using standard pulses delayed fluorescence analysis methods. The obtained results showed that the model was able to separate particles in the fields of low- and high-energy transfer.

Keywords: radiation particle discrimination, ANN, machine learning, scintillation detectors

1. Introduction

Neutron detection is one of the most important tasks in neutron spectroscopy studies and in the design and construction of setup for neutron shielding. Scintillation detectors are most suitable in the field due to their ability to register the spectrum and determine the particle type independently of neutron energy, whereas gaseous ^3He detectors are much more effective in the region of thermal neutron energy. Additionally, the ^3He gas itself is expensive due to its low natural abundance and required production from radioactive tritium [1]. A negative feature of scintillation detectors is their sensitivity to gamma radiation, thus impulses induced by gamma photons are unavoidable when recording neutron flux, because of the nature of neutrons. As a result, the accuracy of the detectors decreases when neutrons are record-

ed. Pulse shape discrimination (PSD) methods are used to distinguish neutron-induced pulses [2–4]. PSD can be applied due to the delayed fluorescence most seen in organic scintillators, anthracene being one of the most popular organic crystals usable for this purpose [5]. Light is likely to be emitted via the triplet–triplet annihilation (TTA) energy relaxation mechanism when heavy ionizing radiation particles lose energy in organic scintillator detector material [6]. Singlet excitation state relaxation provides a prompt and major part of emitted scintillation light. Due to TTA, part of the light is emitted late, resulting in delayed fluorescence.

The common PSD methods are the ratio of delayed fluorescence intensity with the prompt fluorescence component comparison, the rise time and the zero-crossing methods. Comparison of a delayed fluorescence integral with a full pulse integral is used most often.

The scintillation light enters the photomultiplier, where it is converted to electrons because of the photoelectric effect. After the secondary emission of electrons in the phototube, the total charge is converted into an electrical pulse. The pulse is digitized via the ADC converter. The results are used in further analysis.

The separation quality of neutrons and gamma ionizing radiation is described by the figure of merit (FOM) parameter. The FOM parameter is defined as a distance between two different types of pulses in a specific energy range, divided by the sum of the full width at half maximum (FWHM) of the PSD ratio of pulses [7]. The higher the FOM parameter, the better the separation of the pulse induced by neutrons and gamma radiation particles. When the FOM parameter becomes <1 , the separation becomes inaccurate. In this case, only the probability that the particle is determined correctly can be assessed because the normal Gaussian distributions overlap. The particle separation quality of scintillation detectors depends not only on the detector materials, amplification circuit electronics, or the ADC converter but also on the analytical methods. Because of that ML opens new possibilities in this field by analysing each particle charge event. ML models are already used to analyse different electronic pulses and to detect low-intensity pulses in the background of high noise [8]. Support vector machines (SVM) were used before to increase the accuracy of particle discrimination using organic scintillators in a low-energy area [9]. It was shown that SVM methods can provide better accuracy in charge integration than the PSD method.

Several machine learning methods were compared in Ref. [10]. The results of methods have demonstrated superior performance in the classification of nuclear reactions (${}^6\text{Li} + n$).

An application of models usually consists of several stages: selection of a suitable algorithm and preparation of its code, training of model parameters using a training data set, evaluation of test data in the algorithm, evaluation of model accuracy and improvement of the model algorithm for better results. The results presented in this work were obtained by analysing the shape of pulses induced by ionizing radiation using an artificial neural network model.

2. Materials

Polyethylene naphthalate (PEN) is a plastic suitable for use as a scintillation detector that does not require additional wavelength shifting dyes [11]. The maximum photoluminescence of this material depends on the luminescent molecules – excimers. The PEN used in the experiments was obtained from a research group at the Max Planck Institute. Polymer preparation and melting technologies are described in Ref. [12]. The physical parameters of the obtained samples are provided in Table 1.

Table 1. Physical and optical parameters of the obtained samples of polyethylene naphthalate (PEN).

Parameter	Value
Width	30 mm
Length	30 mm
Thickness	3 mm
Density	1.33 g/cm ³
Refractive index	1.62

The photoluminescence peak of PEN is at 445 nm, the spectral measurements were performed using a *Thermo Scientific* Evolution 220 spectrometer. This material has the properties required for the separation of ionizing radiation because part of the scintillation light emitted after the interaction with the particle is from the TTA energy relaxation process. The shape of pulses varies depending on the type of particle that hits the scintillation detector material. In the case of an interaction with a heavy ionizing radiation particle such as an alpha particle or a recoil proton (because of neutron interaction with matter), the ratio between the delayed fluorescence integral and the total pulse integral is higher than during the interaction with the light ionizing radiation particle, e.g. beta or gamma. The examples of normalized pulses induced by averaged alpha and beta particles are given in Fig. 1. The pulses for Fig. 1 were obtained after the PEN exposure to alpha and beta sources, ${}^{238}\text{Pu}$ ($E_{\text{max}} = 5.5$ MeV) and ${}^{90}\text{Sr}/{}^{90}\text{Y}$ ($E_{\text{max}} = 2.2$ MeV), respectively. The plot shows that pulses differ in the delayed fluorescence pulse region. The pulse shape difference of neutrons and gammas is similar to that of alphas and betas, differences are explained in the analysis chapter.

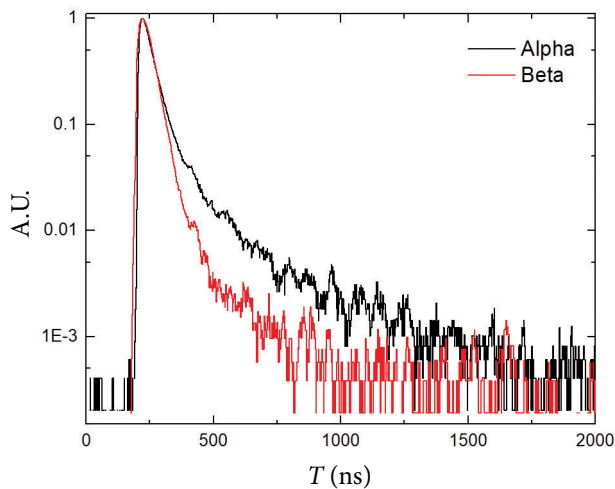


Fig. 1. Shapes of the averaged pulses example obtained after the PEN exposure to alpha (^{238}Pu ($E_{\text{max}} = 5.5 \text{ MeV}$)) and beta ($^{90}\text{Sr}/^{90}\text{Y}$ ($E_{\text{max}} = 2.2 \text{ MeV}$)) sources. Each shape is equal to 250 averaged pulses.

3. Experimental setup

The experimental scheme is shown in Fig. 2. PEN detector scintillation light pulses caused by ioniz-

ing radiation particles were recorded by a *Hama-matsu* photomultiplier (H11934-300) with an active window of $23 \times 23 \text{ mm}$. The photomultiplier is powered by a high-stability, *Ortec* 556 high-voltage source using -700 V voltage. The pulses from the photomultiplier are amplified in a preamplifier and recorded by a *Picoscope* 2206 digital oscilloscope with a resolution of 8 bits and a frequency band of 50 Mhz . The registered pulse window is 2048 ns .

Three data sets were obtained during the experiments: alpha – after the PEN exposure to alpha particle flux ($^{238}\text{PuBe}$ source), beta – after the PEN exposure to beta particle flux ($^{90}\text{Sr}/^{90}\text{Y}$ source) and neutron/gamma – after the PEN exposure to combined neutrons and gamma photon flux (combined $^{239}\text{PuBe}$ and $^{238}\text{PuBe}$ source).

4. Analysis

The essence of neutron detection by a scintillation detector is the energy recording of recoil

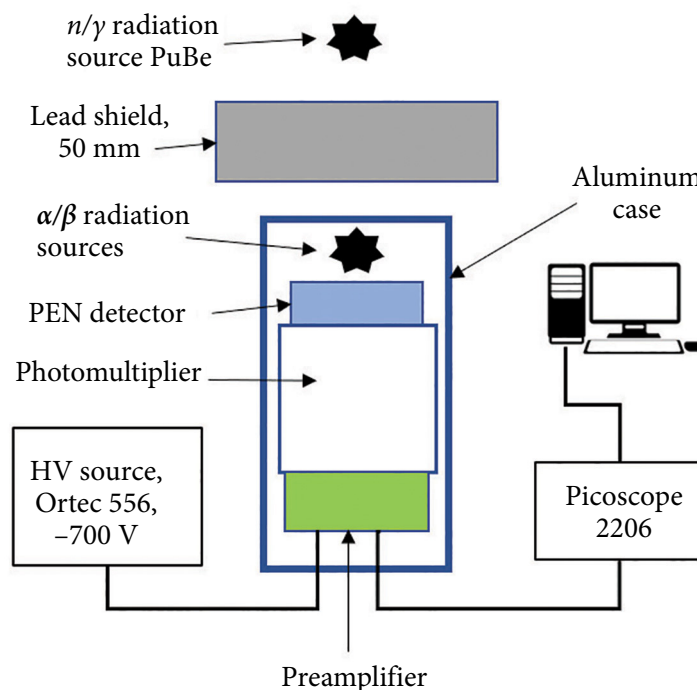


Fig. 2. Schematic of the experimental equipment with the PEN detector and various sources of ionizing radiation used in the experiments. Photomultiplier (PT) was connected to a high voltage power source *Ortec* 556. *Picoscope* 2206 was used as an analog-digital converter (ADC) and data analyzer. The PT and amplifier were mounted in an aluminum case and the PEN was mounted on the PT optical input window ($23 \times 23 \text{ mm}$).

protons in the detector material. Neutrons, similarly to gamma radiation photons, are recorded via the secondary particles, i.e. in both cases analysed pulses are derived from the secondary particles. In the case of interaction with the gamma radiation photon, the interaction of secondary electrons (Compton and photoelectric effect) with the detector is analysed, while in the case of neutron interaction, the interaction of recoil protons is analysed, that is similar to the interaction of the alpha particle with the detector material. The pulse analysis using a comparison of the delayed (Q_D) and total pulse integral (Q_T) is plotted in Fig. 3. Here, neutron-induced pulses are plotted in the right part of the graph and gamma in the left part.

As shown in Fig. 3, from a certain threshold ($Q_T < 15000$), it becomes undefined what type of particle hits the detector as the areas overlap. From that limit, it is possible to determine only the statistical probability of a specific type of ionizing radiation particle interacting with the detector material. As the energy left by the particle in the detector material decreases, separation errors increase and the accuracy of the particle determination decreases.

An artificial neural network was used to determine the type of particles and to increase the accuracy of detection. Models were developed in the Knime analytics platform [13] environment using python Keras (version 2.2.4) and TensorFlow (version 2.2.0) software packages.

The model was made using 3 Keras network layers (an input layer, a first dense layer with Tanh activation function and a second dense layer with a Sigmoid activation layer). Cross validation was applied to the model to fine-tune parameters, such as the number of the first dense layer output units (8 was used as optimal). Other combinations and the quantity of layers did not noticeably improve the quality of the model. The Keras network learner was trained using a maximum of 100 epochs (or till the loss function reaches plateau conditions) with 200 training batches and 200 validation batches. The optimizer was set to Adam with a learning rate equal to 0.001. The binary cross entropy function was used as a loss function in the learning process. A validation data set was used to calculate the loss function value on each epoch.

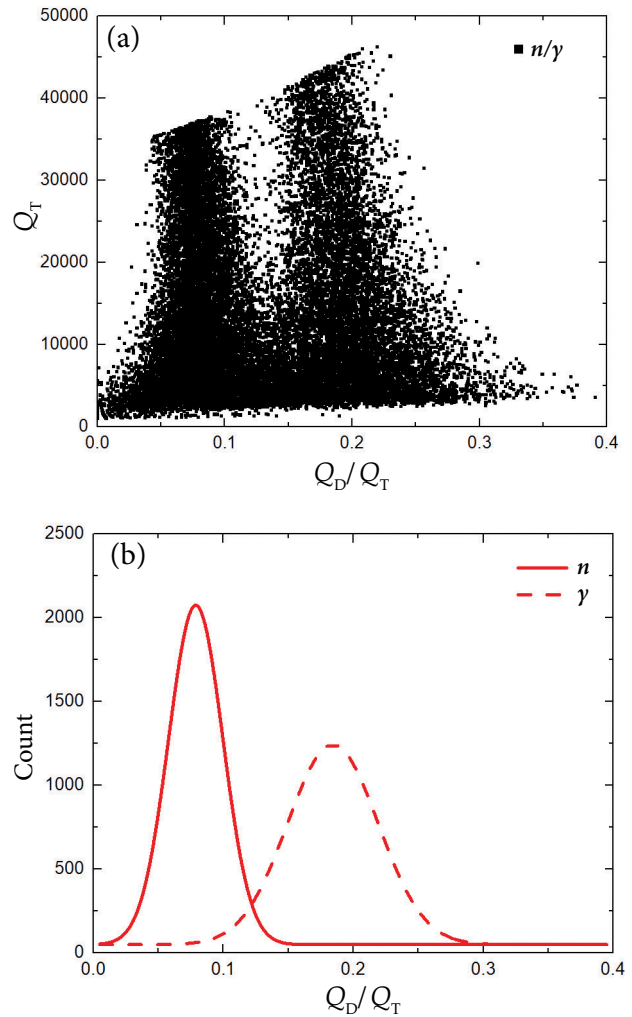


Fig. 3. (a) Total pulse (Q_T) integral versus delayed fluorescence and the total pulse integral ratio (Q_D/Q_T) for neutrons and gamma rays of the PEN detector sample. Gammas are in the left part of the graph because of lower delayed fluorescence intensity. Data was truncated on $Q_T > 35000$ because of the limits of the registration maximum voltage window in ADC. Pulses were registered using a 3 mm PEN detector. (b) Dashed and continuous lines stand for normal Gauss pulses distribution of the total pulse (Q_T) integral versus delayed fluorescence and the total pulse integral ratio (Q_D/Q_T) for neutrons and gamma rays.

5. Data preparation and model training

Data cleaning was applied before training. Cleaning is needed because it is not possible to ensure data reliability due to natural gamma radiation and high-energy cosmic neutron radiation which gives false results.

Models were trained using combined alpha and beta and prepared for training neutron/gamma radiation pulse data sets. The data set of

neutron/gamma radiation training contained cleaned and filtered [$Q_T > 15000$] pulse information. As mentioned before, neutron/gamma separation information under that threshold is not accurate enough (Fig. 3). Data sets of alpha and beta pulses were chosen for the reliability of their data in the low-energy field. The filtered neutron/gamma data set was used because alpha and beta data sets do not provide enough information in the high-energy area [$Q_T > 20000$].

A comparison of the total and delayed fluorescence integrals of used data sets is presented in Figs. 4 and 5.

The data set (76000 pulses) was divided into three parts: training (70%), testing (24%) and validation (6%) sets.

Whole pulse transient data, as shown in Fig. 1, was used to model training. Each pulse length was equal to 1,024 data points. Before training models, the data was scaled within the limits of each pulse to eliminate possible bad decisions on the absolute value of the pulse height. A trained and tested model was used to determine neutron and gamma ionizing radiation particles from a raw data set obtained by recording the total neutron and gamma flux from a $^{239}\text{PuBe}$ and $^{238}\text{PuBe}$ source.

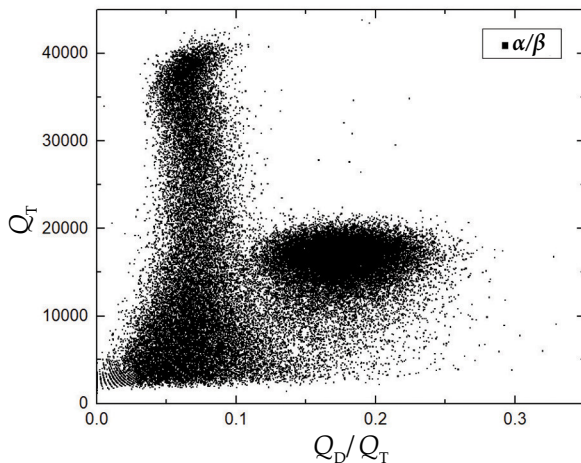


Fig. 4. Delayed fluorescence and total integrals ratio (Q_D/Q_T) versus the total integral (Q_T) for α and β ionizing particles irradiation. Data was obtained after the PEN exposure to alpha and beta sources independently. α is ^{238}Pu ($E_{\text{max}} = 5.5$ MeV) and β is $^{90}\text{Sr}/^{90}\text{Y}$ ($E_{\text{max}} = 2.2$ MeV). α ionizing radiation particles are in the upper part of the graph and β particles are in the lower part. Pulses were registered using a 3 mm PEN detector. Represented data were used for model training.

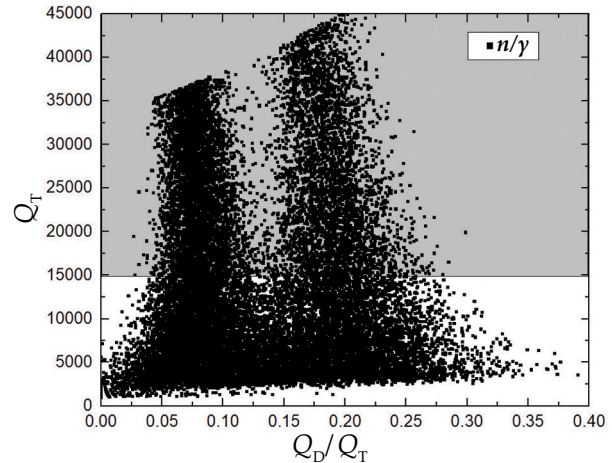


Fig. 5. Delayed fluorescence and total integrals ratio (Q_D/Q_T) versus the total integral (Q_T) for neutron and gamma ionizing particle radiation. Data was obtained after the PEN exposure to combined neutron and gamma flux (combined $^{239}\text{PuBe}$ and $^{238}\text{PuBe}$ source). Neutrons are in the upper part of the graph and gamma particles are in the lower part. Pulses were registered using a 3 mm PEN detector. Data was truncated on $Q_T > 35000$ because of the limits of the registration maximum voltage window in ADC. Highlighted gray area marks the data part that was used for model training.

6. Results

Figure 6 shows the initial ROC results using the test data set, the area under the curve value equal to 0.98. The area under the ROC curve directly represents the quality of the neutron/gamma discrimination in the test data set.

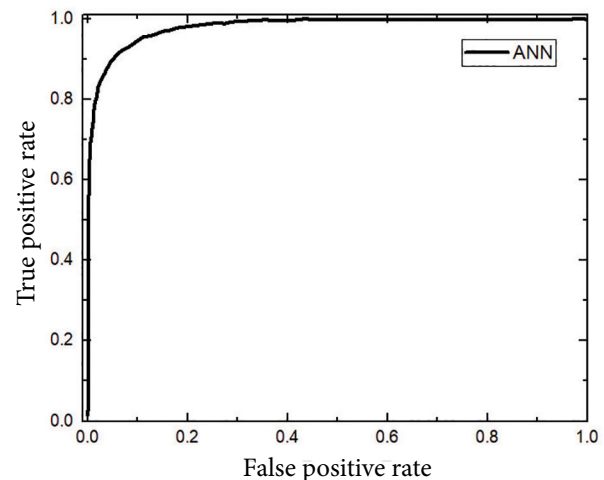


Fig. 6. ROC curve of the trained ANN model. The area under the curve is equal to 0.98. Results were obtained using a test data set.

Raw (not cleaned but normalized) pulse data obtained by recording the total neutron and gamma flux were grouped by a neural network. The results are represented in Fig. 7. Graphs are showing how the proposed model can determine the type of interacting ionizing radiation particles. However, reliable data are obtained only in the energy domain where the verification of separation of particles is possible using mathematical impulse integral comparison methods such as a comparison of Q_T and Q_D integrals. The models determine the type of radiation in the low-energy field, but there are currently no tools to guarantee the reliability of the information. Figure 8 shows the difference between the raw

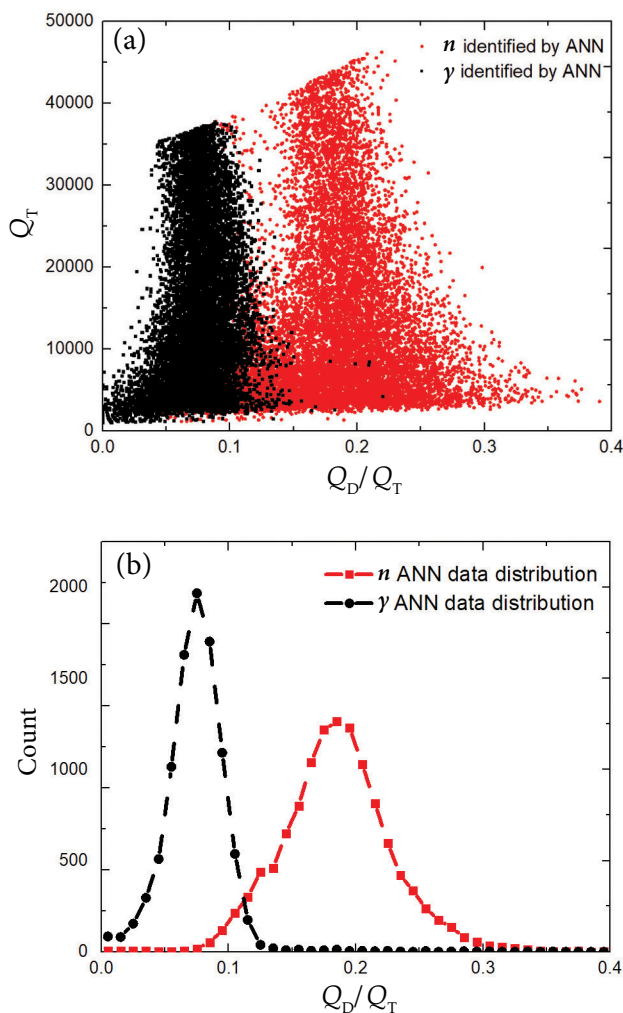


Fig. 7. (a) Neutrons (red) and gammas (black) pulses grouped by the artificial neural network model. (b) Lines stand for the pulses grouped by artificial neural network distribution. Initial data was truncated on $Q_T > 35000$ because of the limits of the registration maximum voltage window in ADC.

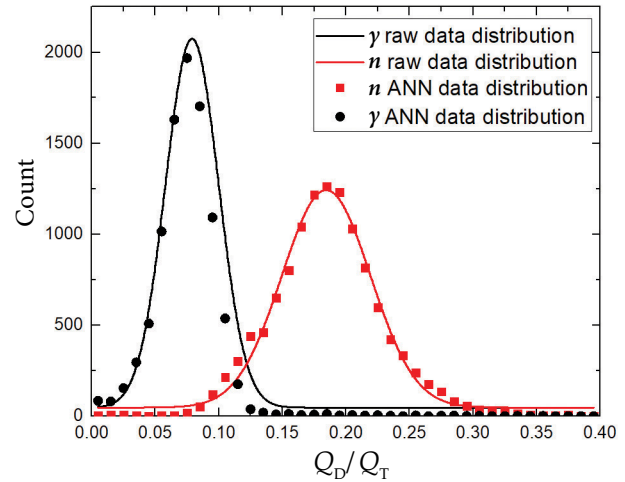


Fig. 8. Comparison of raw pulse integral normal distribution with pulse integrals grouped by the artificial neural network model. Raw data are represented as lines grouped by ANN as symbols.

data Gaussian distribution and grouped data by ML. It is clear from the graph that distributions are mostly matching and the biggest mismatches are in the 0.1–0.13 integral ratio area. The mentioned area is the region where neutron and gamma pulse integrals are starting to overlap, and it is the most difficult area from a statistics perspective as probabilities of true positive decisions are based on real neutrons and gamma proportion. ML is selecting more neutrons than the normal distribution shows in that region.

7. Conclusions

The proposed ANN network provides superior performance in the test data set classification. Moreover, the model provides a correct pulse grouping in the high-energy region; however, in the low-energy region more mismatches from the normal distribution appear. Based on a comparison of the statistical model response distribution and raw data normal distribution, it can be stated that the model is statistically correct, although it cannot be stated for each pulse in the low-energy range. Additional models and data preparation methods are needed to increase model accuracy in low-energy regions.

References

- [1] R. Kouzes, J. Ely, A. Lintereur, E. Siciliano, D. Stromswold, and M.L. Woodring, *^3He Neutron*

- Detector Pressure Effect and Comparison to Models* (Pacific Northwest National Lab. (PNNL), Richland, WA, United States, 2010), <https://doi.org/10.2172/971884>
- [2] M. Grodzicka-Kobylka, T. Szczesniak, L. Swiderski, K. Brylew, M. Moszyński, J. Valiente-Dobón, P. Schotanus, K. Grodzicki, P. Mazerewicz, J. Szymanowski, and Z. Mianowska, Comparison of detectors with pulse shape discrimination capability for simultaneous detection of gamma-rays, slow and fast neutrons, *Nucl. Instrum. Methods Phys. Res. A* **1019**, 165858 (2021), <https://doi.org/10.1016/j.nima.2021.165858>
- [3] G.H.V. Bertrand, M. Hamel, S. Normand, and F. Sguerra, Pulse shape discrimination between (fast or thermal) neutrons and gamma rays with plastic scintillators: State of the art, *Nucl. Instrum. Methods Phys. Res. A* **776** (2015), <https://doi.org/10.1016/j.nima.2014.12.024>
- [4] P.N. Zhmurin, V.N. Lebedev, A.F. Adadurov, V.N. Pereymak, and Yu.A. Gurkalenko, Plastic scintillator for pulse shape neutrons and gamma quanta discrimination, *Radiat. Meas.* **62**, 1–5 (2014), <https://doi.org/10.1016/j.radmeas.2013.12.013>
- [5] T. Yanagida, K. Watanabe, and Y. Fujimoto, Comparative study of neutron and gamma-ray pulse shape discrimination of anthracene, stilbene, and p-terphenyl, *Nucl. Instrum. Methods Phys. Res. A* **784**, 111–114 (2015), <https://doi.org/10.1016/j.nima.2014.12.031>
- [6] P. Blanc, M. Hamel, L. Rocha, S. Normand, R. Pansu, F. Gorbart, and I. Lampre, in: *Proceedings of 2013 3rd International Conference on Advancements in Nuclear Instrumentation, Measurement Methods and Their Applications* (Marseille, France, 2013) pp. 1–9, <https://doi.org/10.1109/ANIMMA.2013.6727919>
- [7] W.G.J. Langeveld, M.J. King, J. Kwong, and D.T. Wakeford, Pulse shape discrimination algorithms, figures of merit, and gamma-rejection for liquid and solid scintillators, *IEEE Trans. Nucl. Sci.* **64**(7), 1801–1809 (2017), <https://doi.org/10.1109/TNS.2017.2681654>
- [8] L. Su, L. Deng, W. Zhu, and S. Zhao, Statistical detection of weak pulse signal under chaotic noise based on Elman neural network, *Wirel. Commun. Mob. Comput.* **2020**, 1–12 (2020), <https://doi.org/10.1155/2020/9653586>
- [9] T.S. Sanderson, C.D. Scott, M. Flaska, J.K. Polack, and S.A. Pozziet, in: *Proceedings of 2012 IEEE Nuclear Science Symposium and Medical Imaging Conference Record (NSS/MIC)* (2012) pp. 199–202, <https://doi.org/10.1109/NSSMIC.2012.6551092>
- [10] J. Griffiths, S. Kleinegesse, D. Saunders, R. Taylor, and A. Vacheret, Pulse shape discrimination and exploration of scintillation signals using convolutional neural network, *Mach. Learn. Sci. Technol.* **1**(4), 045022 (2020), <https://doi.org/10.1088/2632-2153/abb781>
- [11] J. Garankin, A. Plukis, R. Plukienė, E. Lagzdina, and V. Remeikis, Identification of particles of ionizing radiation by the analysis of fluorescence pulse form of the thin pen film scintillator, *IEEE Trans. Nucl. Sci.* **65**(2), 739–743 (2018), <https://doi.org/10.1109/TNS.2017.2785683>
- [12] Y. Efremenko, L. Fajt, M. Febbraro, F. Fischer, C. Hayward, R. Hodák, T. Kraetzschar, B. Majorovits, D. Muenstermann, E. Öz, et al., Use of polyethylene naphthalate as a self-vetoing structural material, *arXiv:1901.03579* (2019), <https://arxiv.org/abs/1901.03579v2>
- [13] F.V. Ordenes and R. Silipo, Machine learning for marketing on the KNIME Hub: The development of a live repository for marketing applications, *J. Bus. Res.* **137**, 393–410 (2021), <https://doi.org/10.1016/j.jbusres.2021.08.036>

DIRBTINIO NEURONINIO TINKLO TAIKYMAS JONIZUOJANČIOSIOS SPINDULIUOTĖS DALELĖMS IDENTIFIKUOTI PAGAL PLASTIKINIO SCINTILIACINIO DETEKTORIAUS ATSAKĄ

J. Garankin, A. Plukis

Fizinių ir technologijos mokslų centras, Vilnius, Lietuva

Santrauka

Jonizuojančiosios spinduliuotės dalelių atskyrimas – svarbi ir sudėtinga užduotis, ypač neutronų ir gama spindulių atžvilgiu. Neutronų ir gama spinduliuotės atskyrimas yra būtinas radiacinės saugos tikslais ir branduolinių reakcijų kontrolei. Standartiniai matematiniai impulsų analizės modeliai gerai veikia, esant didelei dalelės energijos perdavai (>1 MeV). Atskyrimo kokybė prastėja mažėjant perduodamos energijos kiekiui, todėl neįmanoma nustatyti tikslaus dalelės tipo, esant gana žemam energijos perdavos lygiui.

Šiame darbe buvo panaudotas dirbtinio neuroninio tinklo modelis, sprendžiant atskyrimo, esant žemai energijos perdavai, problemą. ML (mašininio mokymosi) modelis buvo naudojamas analizuojant impulsus,

gautus iš PEN (polietileno naftalato) scintiliacinio detektoriaus. Dirbtinio neuroninio tinklo modeliams mokytis buvo naudojami duomenų rinkiniai, gauti veikiant PEN detektorius alfa (^{238}Pu šaltinis), beta (^{90}Sr / ^{90}Y šaltinis) ir kombinuotu neutronų ir gama fotonų ($^{239}\text{PuBe}$ ir $^{238}\text{PuBe}$ šaltinių mišinys) srautais. Neuroninio tinklo atsako duomenys buvo lyginami su standartiniais matematiniais jonizuojančiosios spinduliuotės atskyrimo būdais, kuriuose naudojamas greitosios ir uždelstosios fluorescencijos santykis. Gauti rezultatai parodė, kad modelis sugeba labai gerai atskirti daleles didelės energijos perdavos srityje, taip pat jis identifikuoja daleles ir mažos energijos perdavos srityje, tačiau nėra įrankių, leidžiančių patikrinti rezultatų patikimumą.